# Research on Speckle Classification of Multimode Fiber Based on Inception V3

**Zifei Li** ( 212573062@st.usst.edu.cn )
University of Shanghai for Science and Technology
**Zili Zhang**
Huazhong University of Science and Technology
**Leihong Zhang**
University of Shanghai for Science and Technology
**Runchu Xu**
University of Shanghai for Science and Technology
**Dawei Zhang**
University of Shanghai for Science and Technology

**Research Article**

**Keywords:**

**Posted Date:** May 9th, 2022

**DOI:** https://doi.org/10.21203/rs.3.rs-1615841/v1

# Research on Speckle Classification of Multimode Fiber Based on Inception V3

**Zifei Li[1], Zili Zhang[2],Leihong Zhang[1],Runchu Xu[3],Dawei Zhang[3]**

*[1]College of Communication and Art design, University of Shanghai for Science and Technology, Shanghai 200093, China*

*[2]School of Computer Science and Technology, Huazhong University of Science and Technology, No. 1037, Luoyu Road, Hongshan Dist., Wuhan 430074, China*

*[3]School of Optical-Electrical and Computer Engineering, University of Shanghai for Science and Technology, Shanghai 200093, China.*

**Abstract:**Multimode fibers(MMF) play a crucial role in promoting the miniaturization of endoscopes. With the development of deep learning and machine learning, neural networks can be used to recognize and classify the speckle patterns obtained at the output of optical fibers. Based on the speckle pattern of HERLEV cell images transmitted by multimode fiber, this paper studies the recognition accuracy of support vector machines (SVM), k-nearest neighbors (KNN) and convolutional neural networks (Inception V3) for multiple types of speckle. The experimental results show that Inception V3 has the highest classification accuracy, which is 1.60% and 0.58% higher than the classification accuracy of SVM and KNN algorithms on 7 types of cervical cell data sets respectively, reaches 97.9% accuracy, confirming the effectiveness of Inception V3 algorithm in identifying speckle.

## 1 Introduction

In the field of biomedicine, endoscopes play an important role in interventional medicine. Optical fibers are flexible and can be bent. Therefore, the miniaturization of endoscopes using optical technology has become the main research direction [1-3]. Compared with fiber bundle endoscopes, MMF can transmit multiple light modes due to its larger core diameter, which is an excellent choice for promoting the miniaturization of endoscopes. However, as a special scattering medium, the light mode transmitted through MMF is unstable and affected by multi-mode dispersion, which leads to the target information being disturbed into speckles [4]. In order to identify the speckle pattern at the far end of the multimode fiber, phase conjugation, wavefront shaping and fiber transmission matrix calculation were used to recover and identify the speckle pattern at the far end of multi-mode fiber. However, these methods required accurate calibration and repeated measurement, and had certain limitations in flexibility and stability.

With the rapid development of deep learning technology, the use of convolutional neural network (CNN) to identify speckle patterns at the far end has become the latest solution. In 2017, Ryosuke Takagi et al. compared the three supervised learning methods of support vector machine, adaptive enhancement and neural network based on CBCL data set (face/non-face images), and the classification accuracy reached about 90% [9]. In 2018, Borhani N et al. used U-NET model to reconstruct the input image, and then used CNN to classify the light spots of 10 digits input at the input end, achieving an accuracy rate of about 98% [10]. In the same year, Wang et al. improved the classification accuracy of CBCL data sets by combining AlexNet model and support vector machine [11]. In 2019, Kakkava E et al studied the effects of MMF length, speckle type (amplitude, phase, hologram, etc.) and speckle drop sampling on classification accuracy of

MNIST dataset based on VGG network [12]. Due to the influence of many external factors in the transmission of optical signals of multi-mode fiber, the speckle pattern collected at the output end fluctuates greatly, which increases the difficulty of multi-classification processing, but the neural network can still reconstruct and classify noisy signals.

This paper studies the recognition accuracy of support vector machines (SVM), k-nearest neighbors (KNN) and convolutional neural networks (Inception V3) for multiple types of speckle. According to the experimental results, the classification accuracy and running time of each algorithm are calculated to evaluate the speckle recognition performance of different algorithms.

## 2 Theoretical basis

### 2.1 The principle of multimode fiber imaging

In an optical system, when the optical field and the optical element do not produce nonlinear effects, the relationship between the input signal and the output signal of the optical system can be described by a system function. For the speckle image output by the multimode fiber, the incident light at the input end of the multimode fiber and the light transmitted to the output end can be defined as a fixed number of propagation vectors that are orthogonal to each other between different modes, then the input light field and the output light field It can be expressed as Eq.(1):

$$E_m^{out} = \sum_n t_{mn} E_n^{in} \tag{1}$$

Where $E_m^{out}$ is the output light field, $E_n^{in}$ is the input light field, and $t_{mn}$ is the complexity of the nth input mode and mth the output mode [13]. According to the current development status, the main multimode fiber imaging methods are divided into phase conjugation and digital iterative methods. The phase conjugation is further divided into analog phase conjugation and digital phase conjugation. An experimental platform can be built for each input. The intensity, amplitude and phase of the pattern and output speckle are measured [14], and the complex matrix is set according to the experimental data to realize the function of information transmission.

As shown in Fig.1, the process is a schematic diagram of multi-mode fiber imaging. The laser emits laser light as an optical carrier, combined with a polarized beam splitter and a half-wave plate, and a reflective spatial light modulator is used to transmit grayscale image information to the optical carrier. On the optical path, the optical carrier carries the optical information of the grayscale image. An objective lens is used at the input end of the fiber to couple the image information into the multimode fiber, and the same objective lens is used at the output end of the fiber to couple the image information out of the multimode fiber to complete the information transmission in the multimode fiber. Speckle at the output of the fiber is collected by an imaging lens and then imaged onto a CMOS camera.

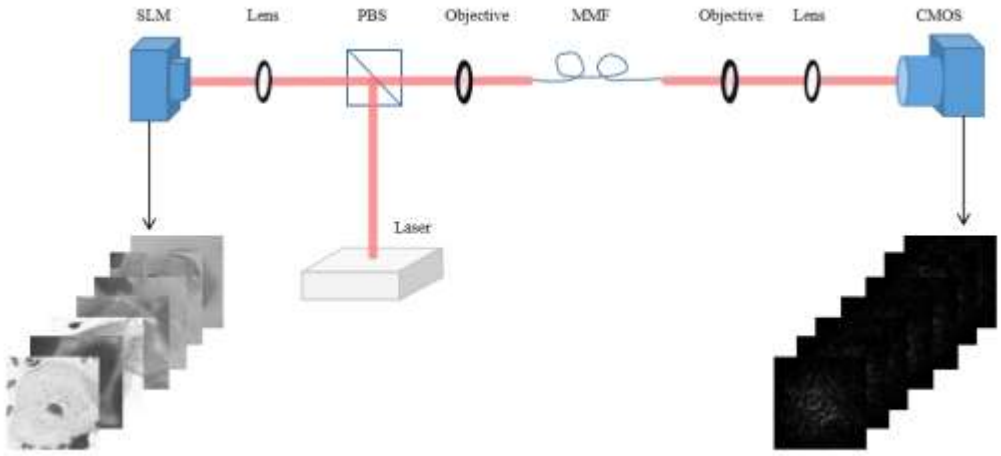


**Fig.1** Schematic diagram of multimode fiber imaging

**2.2 Support vector machines**

Support vector machines [15,16] are a supervised learning algorithm applied to data classification. As shown in Figure 2, the basic idea of SVM is to construct the separation hyperplane with the largest margin between the two types of sample sets. The support vector machine finds a classifier to maximize the boundary between the hyperplane and the sample, and the hyperplane with the largest boundary is the optimal classifier that the support vector machine finds.

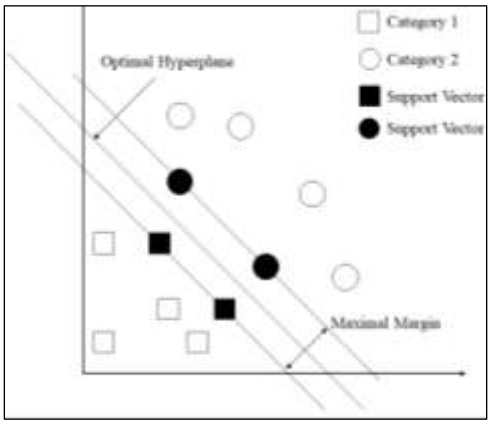


**Fig.2** SVM binary classification calculation principle diagram

There is a straight line that can separate two different samples, and make this straight line satisfy the constraints of Eq.(2) and Eq.(3):

$$w^T x+b\geq+1,\ y_i=1 \tag{2}$$

$$w^T x+b\leq+1,\ y_i=-1 \tag{3}$$

The distance between two straight lines is represented by Margin, and its expression is shown in Eq.(4).

$$M\arg in=\frac{2}{\sqrt{\omega^T\omega}} \tag{4}$$

The value of $\omega$ is optimized by maximizing Margin under the constraints. The constant b is equivalent to the intercept of the straight line, which can be obtained according to the mathematical relationship, so that a straight line that can perfectly divide two different samples can be obtained. Then, on this basis, the principle of SVM algorithm for multi-classification is introduced. If the SVM algorithm needs to classify M samples, it is equivalent to a two-class SVM between every two classes. The principle is shown in Fig.3.

Fig.3 shows the classification ideas of three different samples. First, find sample A and sample B for binary classification. The principle is the same as that described in Fig.1. At the same time, sample B and sample C, as well as sample A and sample C, should be classified into two categories, so three decision boundaries are obtained. $d_{AB}$ is the

decision boundaries of A and B, $d_{AC}$ is the decision boundary of A and C, and $d_{BC}$ is the decision boundary of B and C. After obtaining the three decision boundaries , a multi-class decision boundary can be obtained according to the constraints and the decision boundary of each binary classification. Figure 2 (a) is the situation before sample classification, and (b) is the situation after classification according to the decision boundary. If the SVM needs to complete a large number of classification types, then it needs to increase the dimension to the multi-dimensional space to construct the decision boundary sort.

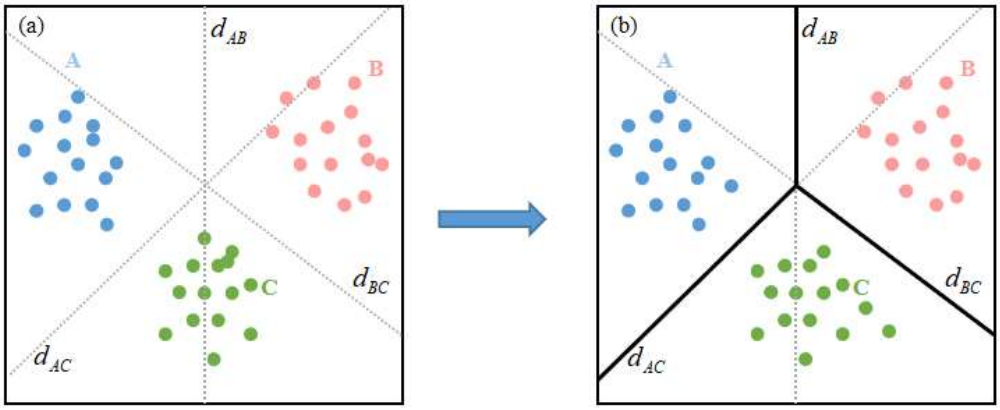


**Fig.3** SVM multi-classification schematic diagram, (a) represents the concept map before classification, and (b) represents the concept map after classification.

### 2.3 K-nearest neighbors

KNN (k-nearest neighbor) [17] is a simple and classic machine learning classification algorithm that classifies samples by measuring the distance (usually Euclidean distance) between “data to be classified” and “samples with known classes”. Figure 4 is the identification principle diagram of the KNN algorithm. The following is a brief introduction to the method and principle of the KNN algorithm.

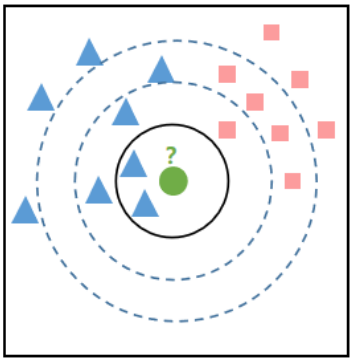


**Fig.4** Schematic diagram of KNN algorithm

As shown in Fig.4, there are two different samples of triangle and square in the sample space, and now a circular point to be classified is added. First, select the K points closest to the sample point around the sample point, then in these K points, classify the new sample into a large number of categories. When selecting K adjacent points, it is necessary to calculate the distance between the circular point to be classified and other surrounding points. Among them, the Euclidean distance is used to calculate more distances. Taking a two-dimensional plane as an example, the calculation formula of the Euclidean distance is as Eq.(5) shown.

$$\rho = \sqrt{(x_2 - x_1)^2 + (y_2 - y_1)^2} \qquad (5)$$

If there are many types to be classified, the dimension is raised to multi-dimensional, then the Euclidean distance calculation formula is

changed to Eq. (6).

$$\rho = \sqrt{\sum_{i=1}^{n} (x_i - y_i)^2} \tag{6}$$

As a common algorithm for machine learning, the biggest advantage of KNN is that it is simple and insensitive to outliers, but the disadvantage is that it needs to give the classification results first, and it cannot perform unsupervised learning. Because the sample points can be mapped to multi-dimensional space for calculation as the number of classification types increases, the KNN algorithm can also identify and classify the output speckle of multimode fiber.

### 2.4 Deep neural network—inception v3 model

The improvement in the accuracy of classification networks in recent years has greatly helped other related machine vision applications, such as face recognition, object detection, etc., because they can all use classification networks to extract features. Although AlexNet [18], VGGNet [19] are very successful, their computational cost is too large and the number of model parameters is large, in contrast, the Inception [20, 21] model not only has a small amount of parameters, but also has strong feature extraction capabilities. During the training phase, the Inception model can avoid excessive compression of feature information in the shallow layers of the network, and the size of the feature map will be moderate. Reduce, the high-dimensional feature information will be processed locally, and the nonlinear activation layer will be gradually added to the network, which will reduce the network parameters and make the training speed faster. At the same time, the spatial aggregation of low-dimensional information will not lead to the reduction of network expression ability. Therefore, when performing large-scale convolutions, the input can be dimensionally reduced first, and then the spatial aggregation operation can be performed.

Since Google proposed the Inception model in 2014, it has successively developed five generations of classification models including Inception-Resnet, which design 1*1 convolution, 3*3 convolution, 5*5 convolution and 3*3 pooling through the underlying design. Simplifying the network architecture ensures that each layer of the network structure can learn the target sparse features and increase the network width and depth. The Inception network model is shown in Fig.5(a).

The theory proposed by Szegedy [21] et al. to introduce appropriate decomposed convolution and active regularization to reduce the computational complexity of the target, that is, the advent of Inception V3 has a good performance in both model parameters and computational effort. In terms of structure, Inception V3 continues the network architecture of Inception as a whole, modified the Inception block, replaced 5*5 with multiple 3*3 convolutional layers, replaced 5*5 with 1*7 and 7*1 convolutional layers, replaced 3 *3 is the 1*3 and 3*1 convolutional layers, as shown in Fig.5(b),(c),(d). The convolution decomposition [22] reduces the amount of parameter calculation, and the auxiliary classifier is used as a regularizer, which solves the problem of gradient disappearance and improves the convergence during training. The original large convolution kernel is decomposed into small convolution kernels with the same output. It effectively retains the image features while reducing the amount of computation, decomposes the larger convolution into several smaller convolutions, reduces the amount of parameters and improves the generalization ability under the

premise of ensuring the same effect.

Due to the small size of the HERLEV dataset, inconspicuous features, and few features, we chose the Inception V3 network. Therefore, when using a deep neural network for training, the Inception V3 network can avoid excessive compression of feature information in the shallow layer, making the feature The size of the map is moderately reduced. At the same time, due to the limitation of computing power, the Inception V3 network handles feature information calculation locally, which can reduce network parameters and train faster.

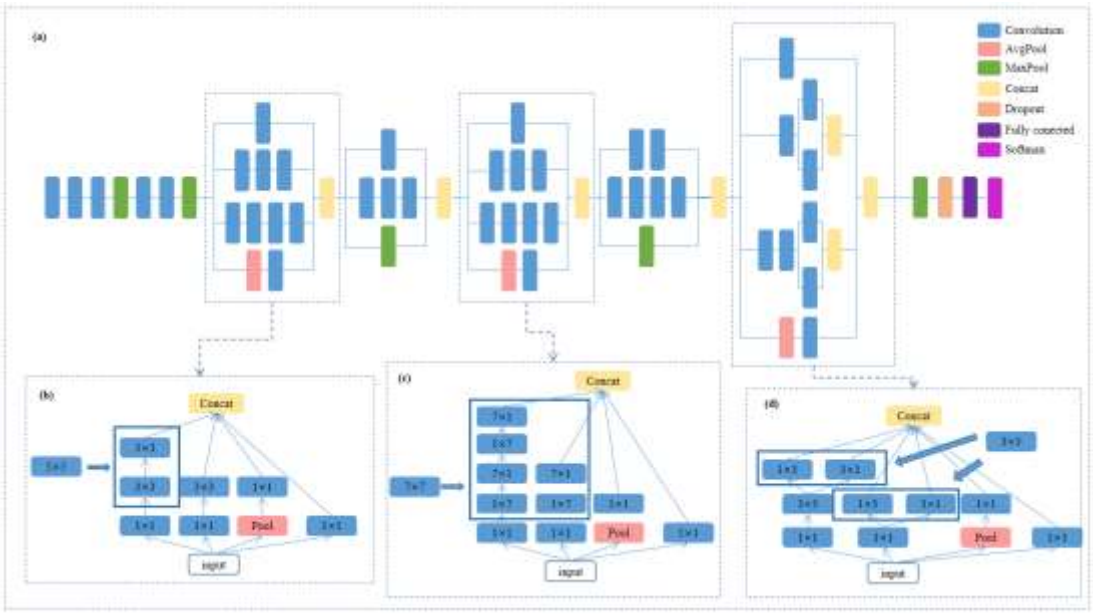

**Fig.5 (a)** Inception network model. **(b)** Inception modules where each 5×5 convolution is replaced by two 3×3 convolution. **(c)** Inception modules after the factorization of the 7×7 convolutions. **(d)** Inception modules with expanded the filter bank outputs.

## 3 Experimental steps and preparation

### 3.1 Experimental steps

Step 1: Selection of datasets. On the basis of existing research, the scene complexity of MNIST, HERLEV and ImageNet datasets is compared, and the rationality of choosing HERLEV dataset is expounded. See Section 3.2 for details.

Step 2: Preprocessing and data augmentation of the HERLEV dataset. See Section 3.3 for details.

Step 3: Using optical experimental system to obtain speckles. Optical system and steps can be seen in section 3.4.

Step 4: Selection of experimental environment (software and hardware) and code parameters. See Section 4.1-4.2 for details.

Step 5: Accuracy and time comparison of SVM, KNN and Inception V3 methods. See section 4.3 for details.

Step 6: Systematically explored the effect of the number of classification categories of the three methods on the accuracy of 7 categories of cervical cell images. See Sections 4.4-4.5 for details.

### 3.2 Experimental dataset

According to existing research [23], for images with simple features, such as the MNIST dataset, the classification accuracy of multi-class handwritten digits is high, and the binary classification based on machine learning has a high recognition accuracy. However, for images with complex scenes,

such as the ImageNet dataset, it is difficult to achieve ideal results. When the number of categories increases, the recognition and classification accuracy of multi-category complex scenes will decrease. The complexity of the HERLEV dataset is between the MNIST dataset and the ImageNet dataset, therefore, we choose the HERLEV dataset to explore the applicability of Inception V3 for speckle classification.

In this paper, we choose 7 types of cervical cell images as the dataset, with a total of 917 images, to study the classification accuracy of SVM, KNN, and Inception V3 for multiple types of speckle. The original image of the dataset and its speckle image are shown in Fig.6.

| | in situ cancer cells | mildly dysplastic cells | moderately dysplastic cells | normal columnar epithelial cells | middle squamous epithelial cells | superficial squamous epithelial cells | severe dysplastic cells |
|---|---|---|---|---|---|---|---|
| HERLEV |  |  |  |  |  |  |  |
| |  |  |  |  |  |  |  |
| Number of samples | 150 | 182 | 146 | 98 | 70 | 74 | 197 |

**Fig.6** Experimental dataset

### 3.3 Dataset preprocess and data augmentation

Considering the small size of the HERLEV dataset and the different sizes and shapes of each image, it is not conducive to optical experiments and machine learning. Therefore, the HERLEV dataset is preprocessed as follows: (1) Grayscale processing and shape change of cervical cell images, as shown in Fig.6. (2) Data enhancement processing. We perform 9 data enhancements on each original image by flipping, translating, shearing, and adding noise to obtain 8253 images as a sample set. An example is shown in Fig.7.

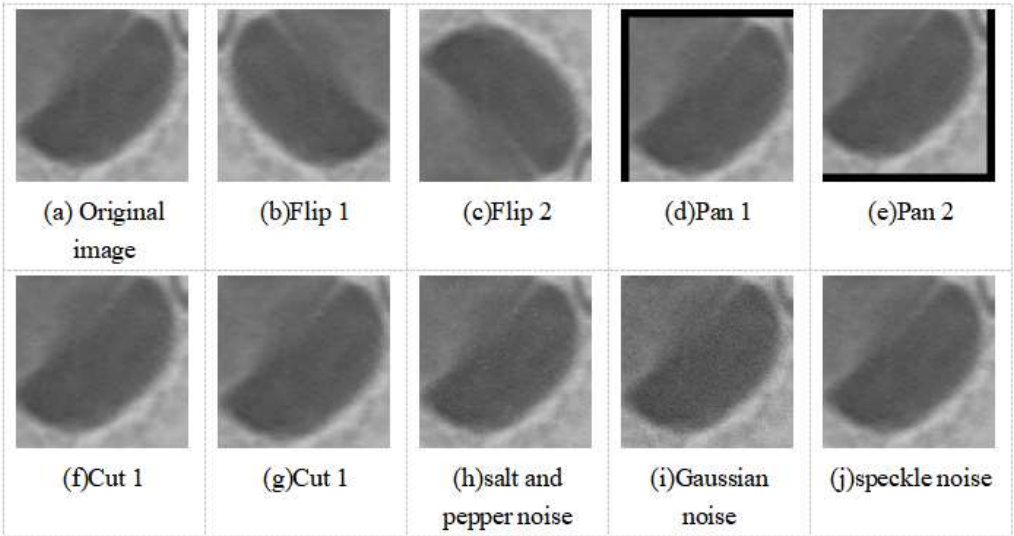


**Fig.7** Dataset Enhancement

### 3.4 Optical system

The optical experiment diagram is shown in Fig.8. The experimental process of obtaining speckles can be described as follows. He-Ne laser emits laser with 632.8nm wavelength as the experimental light source. Focusing, filtering, collimating and expanding the light source by using the micro-objective, pinhole filter and lens1. Using polaroid, beam splitter and spatial light modulator to transmit gray image information to the optical path. The optical information of gray image is coupled into the MMF using objective at the input of fiber, and then the scrambled information is coupled out of the MMF using same objective at the output of fiber, which completes the transmission of optical information in the multimode fiber.The speckles are collected via lens2, and then imaged onto the CCD camera.

Taking the middle squamous epithelial cell as an example, the speckle image obtained after the cell is transmitted by multimode fiber is shown in Fig.9.

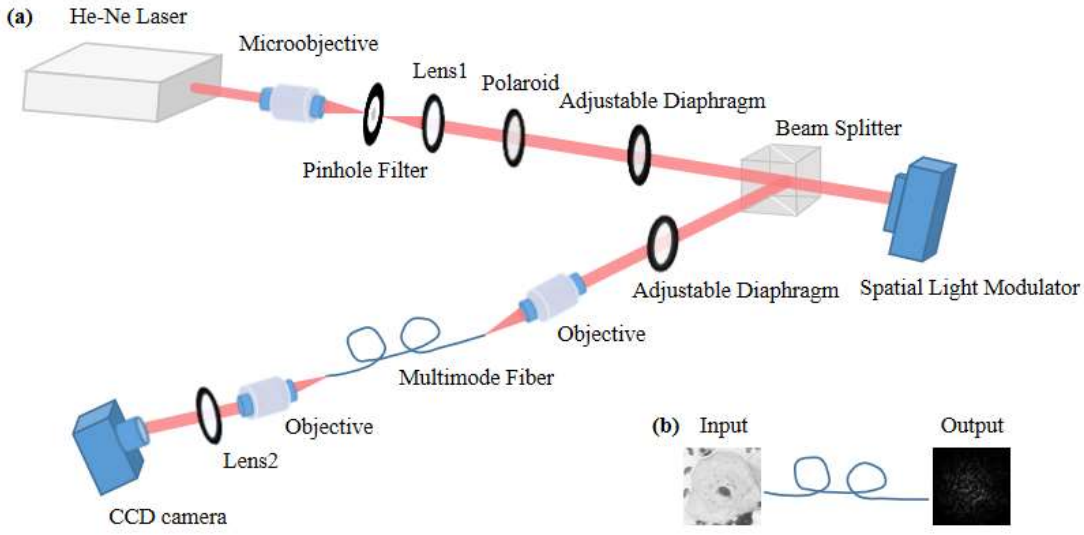


**Fig.8 Optical system (a)** Light Source Wavelength: 632.8nm, Microobjective: magnification, Pinhole Filter: aperture 25 $\mu m$, Lens1: focal length 20cm, Lens2: imaging lens, used to adjust speckle size, focal length 5cm, Spatial Light Modulator: HOLOEYE, Pluto VIS-006, Multimode

Fiber: THORLABS M31L10, graded index fiber, length 10m, core diameter 65 $\mu m$, Adjustable Diaphragm: filter stray light. **(b)** Speckle image obtained by multimode fiber transmission system.

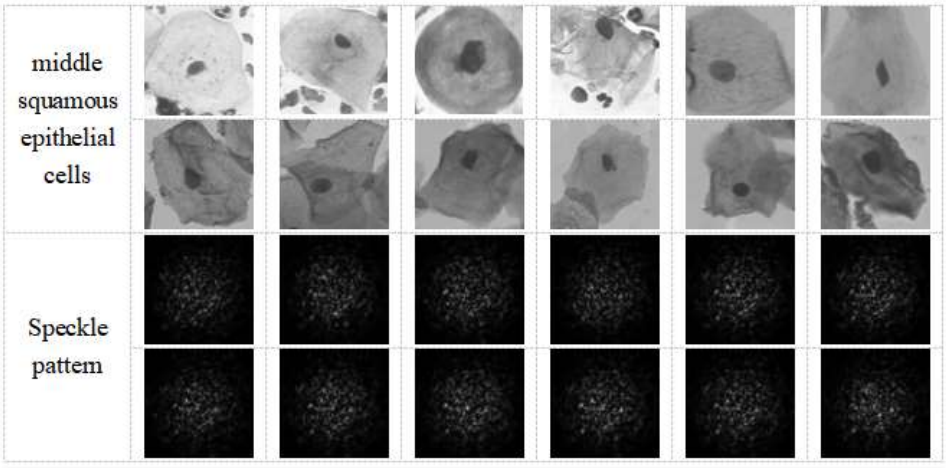


**Fig.9** Speckle pattern

## 4 Simulation experiment and analysis

### 4.1 Environment

Since a large number of convolution calculations are required in model training, the use of GPUs will greatly shorten the training time and speed up the training compared to CPUs. During the experiment, Python was used for development and implementation. The specific hardware environment and software environment description are shown in Table 1.

**Table 1.** Description of experimental environment

| Environment category | project | illustrate |
|---|---|---|
| Hardware environment | CPU | Xeon e5-2640 |
| | GPU | Nvidia GeForce 3090 |
| | RAM | 64GB |
| | hard disk | 256GB |
| Software Environment | operating system | Ubuntu |
| | operating system | Python3.8 |
| | Deep Learning Framework | Tensorflow2.0 |

### 4.2 Parameter setting

(1) The type of support vector machine is C-SVC, the kernel function is the type of linear kernel function, the remaining parameters are default options, and the size of the speckle image is 256×256.

(2) The K value of KNN is 1, the type of the distance formula is correlation distance, the remaining parameters are default options, and the speckle size is 256×256.

(3) The parameters of the Inception V3 experimental model are selected as a learning rate of 0.001, the number of iterations is 50, the batch size (BATCH_SIZE) is 32, the photo

size of the dataset is 256*256, and the activation function is the Relu function. The parameters of the Inception V3 network used in this experiment are shown in Fig.10.

| Layer (type) | Output Shape | Param # |
|---|---|---|
| inception_v3 (Functional) | (None, 6, 6, 2048) | 21802784 |
| dropout (Dropout) | (None, 6, 6, 2048) | 0 |
| batch_normalization (BatchNormalization) | (None, 6, 6, 2048) | 8192 |
| conv2d (Conv2D) | (None, 6, 6, 1024) | 18875392 |
| conv2d_1 (Conv2D) | (None, 6, 6, 1024) | 9438208 |
| max_pooling2d (MaxPooling2D) | (None, 3, 3, 1024) | 0 |
| dropout_1 (Dropout) | (None, 3, 3, 1024) | 0 |
| batch_normalization_1 (BatchNormalization) | (None, 3, 3, 1024) | 4096 |
| flatten (Flatten) | (None, 9216) | 0 |
| dense (Dense) | (None, 1024) | 9438208 |
| dense_1 (Dense) | (None, 7) | 7175 |

**Fig.10** Parameters of the Inception V3 network

In order to evaluate the classification and recognition effect of SVM, KNN, and Inception V3 algorithms, this paper selects the classification accuracy as the evaluation index. The confusion matrix can comprehensively reflect the performance of the model, and many indicators can be derived from the confusion matrix, as shown in Table 2.

**Table 2.** Confusion matrix of binary classification results

| Reality | predict result | |
|---|---|---|
| | True | False |
| True | TP | FN |
| False | FP | TN |

Among them: TP: true example, actual positive prediction is positive; FP: false positive example, actual negative but predicted positive; FN: false negative example, actual positive but predicted negative; TN: true negative example, actual negative prediction is negative. Therefore, the classification accuracy is: Accuracy = (TP+TN) / (TP+FP+TN+FN). When there are more than two classification results, the confusion matrix is applicable at the same time.

### 4.3 Comparison of SVM, KNN, and Inception V3 methods

Take 5278 images as the training set, 1221 images as the validation set, and 917 images as the test set. The test results of the three algorithms obtained are shown in Table 3.

**Table 3.** Test results of three algorithms to identify output speckle of multimode fiber

| Model | Accuracy | Time |
|---|---|---|
| SVM | 95.52% | 0.06s |
| KNN | 96.97% | **0.02s** |
| Inception V3 | **97.90%** | 3.36s |

It can be seen from Table 3 that (1) the classification accuracy of Inception V3 is the highest, reaching 97.9%. Compared with the SVM and KNN algorithms, the classification accuracy of the Inception V3 algorithm on the 7 types of cervical cell data sets is increased by 1.60% and 0.58% respectively. 2) After the

three models are trained, Inception V3 takes longer to test on the test set than SVM and KNN due to the large number of parameters to be learned. (3) The method of using the Inception V3 network has a certain improvement compared with the traditional machine learning method, which confirms the experimental reliability of the classification using the deep neural network Inception V3. Plotting LOSS, AUC curves according to epoch, and seven types of confusion matrix with training AUC metric are shown in Fig.11.

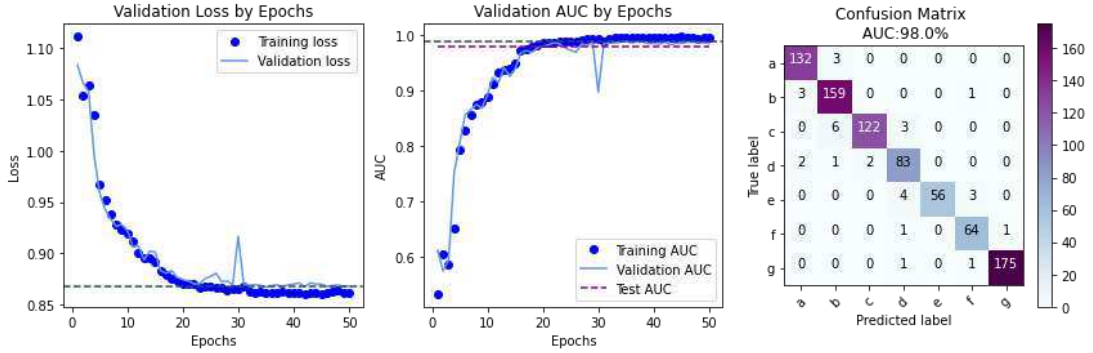


**Fig.11** Experimental result diagram

### 4.4 Comparison of the number of SVM, KNN, Inception V3 categories

Table 4 shows: (1)As the number of categories increases, the classification accuracy gradually decreases. (2) SVM has changed from the original two-classification that only needs to divide one hyperplane to now need to divide multiple hyperplanes. Due to the increase in the number of classifications, it is difficult to select a suitable decision boundary for each class, so the increase in the number of classifications is difficult. time, the accuracy will decrease. (3) KNN needs to select the closest distance to the samples when classifying. When the number of classifications increases, it is difficult for the program to decide which one is its closest sample, so there will be a certain loss in accuracy as the number of classes increases. (4) When the number of categories is small, we find that the two traditional methods, SVM and KNN, perform better, indicating that the traditional classifier has a higher classification accuracy in small category classification. As the number of categories increases, the traditional classification accuracy of the classifier is reduced, and deep learning shows its superiority.

**Table 4** The relationship between the number of categories and the classification accuracy

| Number of categories | 2 | 3 | 4 | 5 | 6 | 7 |
|---|---|---|---|---|---|---|
| SVM | **99.33%** | 97.68% | 96.76% | 95.33% | 95.62% | 95.52% |
| KNN | 98.66% | **98.84%** | **98.30%** | 97.77% | 97.38% | 96.97% |
| Inception V3 | 98.52% | 98.12% | 98.13% | **98.02%** | **97.70%** | **97.90%** |

### 4.5 Comparison of the number of training samples

Table 5 shows: (1) As the number of training samples increases, the classification accuracy also increases. (2) Due to the

increase in the number of samples, the hyperplane of SVM can be divided more clearly and the decision boundary is more obvious, so the accuracy rate can be improved. (3) KNN can better cluster samples when the number of samples increases, so the accuracy rate increases as the number of samples increases. (4) To sum up, in practice, when dealing with multi-class target recognition, usually by expanding the scale of the training set (obtaining more informative features) and improving the accuracy of optical experiments (improving the accuracy of informative features) to fulfill.

Table 5 The relationship between the number of training samples and the classification accuracy

| number of training samples | 200 | 500 | 1000 | 2000 | 3500 | 4000 | 6000 | 8253 |
|---|---|---|---|---|---|---|---|---|
| SVM | **75.42%** | 76.45% | **83.41%** | **93.45%** | 94.41% | 94.45% | 94.69% | 95.52% |
| KNN | 73.61% | **77.69%** | 82.61% | 92.69% | 93.51% | 93.83% | 95.23% | 96.85% |
| Inception V3 | 54.62% | 71.58% | 82.66% | 92.78% | **94.67%** | **96.02%** | **97.11%** | **97.90%** |

## 5 Conclusion

Multimode optical fibers are widely used in the fields of communication and sensing. With the advent of the 5G and 6G era, the requirements for optical fibers and cables in the future communication process will also be higher, and the spot detection technology output by multimode optical fibers will also be applied in In more real-world scenarios, linking the hot machine learning, deep learning and multi-mode fiber imaging detection in the current era can well solve the problem that the multi-mode fiber output cannot be identified or the traditional spot calculation method is too cumbersome.

In this paper, through the experiment of identifying the output speckle pattern of multimode fiber, it is confirmed that the output speckle pattern of multimode fiber can be well identified by neural network. This paper compares the deep learning neural network model with the traditional machine learning algorithm in the classification experiment on the HERLEV data set, that is, the deep neural network Inception V3 method, which has a certain improvement compared to the traditional machine learning method.

## References


[1]. Amitonova L V , Boer J . Endo-microscopy beyond the Abbe and Nyquist limits[J]. light：Science & Applications, 2020, 9(1):12.

[2]. Matthew K, Tomasz ST. Achromatized endomicroscope objective for optical biopsy[J]. Biomedical Optics Express, 2013, 4(2): 287-297.

[3]. Zhang S , Geng T , Niu H , et al. All fiber compact bending sensor with high sensitivity based on a multimode fiber embedded chirped-long period grating[J]. Optics Letters, 2020, 45(15).

[4]. Choi Y, Yoon C, Kim M, et al. Scanner-Free and Wide-Field Endoscopic Imaging by Using a Single Multimode Optical Fiber[J], Physical Review Letters, 2012, 109(20): 203901.

[5]. G J, Dunning, R C, et al. Demonstration of image transmission through fibers by optical phase conjugation.[J]. Optics letters, 1982.

[6]. I M, Vellekoop, A P, et al. Focusing coherent light through opaque strongly scattering media.[J]. Optics letters, 2007.

[7]. Ivo M. Vellekoop 1 ,* and Christof M. Aegerter 1 ,2. Scattered light fluorescence microscopy: imaging through turbid layers[J]. Optics Letters, 2010, 35(8).

[8]. imár, Tomá, Dholakia K . Exploiting multimode waveguides for pure fibre-based imaging[J]. Nature

Communications, 2012, 3(8):1027.
[9]. Takagi R , Horisaki R , Tanida J . Object recognition through a multi-mode fiber[J]. Optical Review, 2017, 24(2):117-120.
[10]. Borhani N , Kakkava E , Moser C , et al. Learning to see through multimode fibers[J]. Optica, 2018, 5(8):960.
[11]. Ping, Wang, Jianglei, et al. Deep learning-based object classification through multimode fiber via a CNN-architecture SpeckleNet.[J]. Applied Optics, 2018.
[12]. Kakkava E , Rahmani B , Borhani N , et al. Imaging through multimode fibers using deep learning: The effects of intensity versus holographic recording of the speckle pattern[J]. Optical Fiber Technology, 2019, 52:101985.
[13]. Popoff S M , Lerosey G , Carminati R , et al. Measuring the Transmission Matrix in Optics : An Approach to the Study and Control of Light Propagation in Disordered Media[J]. Physical Review Letters, 2010, 104(10):100601.
[14]. Mooseok, Jang, Haowen, et al. Relation between speckle decorrelation and optical phase conjugation (OPC)-based turbidity suppression through dynamic scattering media: a study on in vivo mouse skin.[J]. Biomedical optics express, 2015.
[15]. Hearst M A , Dumais S T , Osman E , et al. Support vector machines[J]. IEEE Intelligent Systems & Their Applications, 1998, 13(4):18-28.
[16]. Faruqe M O , Hasan M . Face recognition using PCA and SVM[C]// Anti-counterfeiting, Security, and Identification in Communication, 2009. ASID 2009. 3rd International Conference on. IEEE, 2009.
[17]. Choubey H , Pandey A . A combination of statistical parameters for the detection of epilepsy and EEG classification using ANN and KNN classifier[J]. Signal Image and Video Processing, 2020(5):1-9.
[18]. Krizhevsky A , Sutskever I , Hinton G . ImageNet Classification with Deep Convolutional Neural Networks[J]. Advances in neural information processing systems, 2012, 25(2).
[19]. Simonyan K , Zisserman A . Very Deep Convolutional Networks for Large-Scale Image Recognition[J]. Computer Science, 2014.
[20]. Szegedy C , Liu W , Jia Y , et al. Going Deeper with Convolutions[J]. IEEE Computer Society, 2014.
[21]. Szegedy C , Vanhoucke V , Ioffe S , et al. Rethinking the Inception Architecture for Computer Vision[J]. IEEE, 2016:2818-2826.
[22]. Cao J , Yan M , Jia Y , et al. Application of a modified Inception-v3 model in the dynasty-based classification of ancient murals[J]. 2021.
[23]. Zhang L , Xu R , Wang K , et al. Research on image transmission mechanism through a multimode fiber based on principal component analysis[J]. Optics and Lasers in Engineering, 2020, 134(2):106197.